Chapter 18

Structural Analysis of the Photosystem II Core/Antenna Holocomplex by Electron Microscopy

Ben Hankamer*
Institute of Molecular Bioscience, University of Queensland, St. Lucia, QLD 4072, Australia

James Barber and Jon Nield
Wolfson Laboratories, Department of Biological Sciences, Imperial College London, SW7 2AZ, U.K.

*Author for correspondence, email: b.hankamer@imb.uq.edu.au

T. Wydrzynski and K. Satoh (eds): Photosystem II: The Light-Driven Water:Plastoquinone Oxidoreductase, pp. 403–424.

Summary

Electron microscopy has contributed greatly to the structural biology of Photosystem II (PS II) in higher plants and green algae from the level of its in vivo organization, within the thylakoid membrane, through to the determination of the structure of light-harvesting complex II (LHCII) at 3.4 Å. Freeze-fracture and freeze-etch techniques provided the first visualization of PS II and its antenna systems in vivo. Subsequently a range of PS II and PS II-antenna, super- and mega-complexes were purified from thylakoid membranes using mild detergent solubilization and these were structurally characterized by single particle analysis. In particular these studies showed the structural linkage between the PS II core and a range of bound macromolecular light-harvesting antennae, as well as the overall shape of the extrinsic oxygen-evolving complex. Electron crystallography extended the resolution range, revealing the positioning of PS II subunits and the transmembrane helix organization of both PS II and antenna proteins. This technique also identified many of the chlorin cofactors in the reaction center proteins of D1 and D2, and also in the inner antenna, CP47, and outer antenna of LHCII. Future work will involve obtaining more highly resolved structures of supercomplexes and megacomplexes, using electron cryo-microscopy and including structural information emerging from X-ray and electron crystallography, with the view to gaining a near atomic resolution model of higher plant/green algal PS II as it exists in the native thylakoid membrane.

I. Introduction

In recent years, electron cryo-microscopy (cryo-EM) has developed rapidly in the areas of tomography, single particle analysis and electron crystallography. Cryo-EM tomography has advanced to the stage where a series of tilt images of individual frozen hydrated samples can be used to calculate a 3D reconstruction of organelles and whole cells to a resolution of 5–30 nm. At this resolution individual macromolecular assemblies can be identified, revealing their location, size and shape. This opens up the exciting prospect of being able to fit higher resolution structures, determined by single particle analysis, electron or X-ray crystallography, into the molecular footprints identified within these 3D reconstructions of organelles and whole cells. This combinatorial approach will provide unique insights into the organization and dynamics of macromolecular assemblies, such as Photosystem II (PS II) and its antenna system in vivo.

Single particle analysis lies between cryo-EM tomography and electron crystallography, calculating medium resolution 3D structures of isolated complexes that are randomly oriented in vitreous ice. It is particularly suited to the analysis of large, labile, symmetric macromolecular assemblies, being used in the determination of supermolecular structures of PS II and its antenna system, including the light-harvesting complex (LHCII) system, which have not yet yielded high quality 2D or 3D crystals. 3D reconstructions with a resolution of 7.5–30 Å are now routinely being determined and this range is being extended through a whole array of innovations.

High-resolution electron cryo-crystallography requires large and well-ordered 2D crystals. This approach has to date yielded the highest resolution 3D reconstructions determined by any cryo-EM technique. It is particularly suited for membrane proteins and has yielded structures of LHCII and the PS II core of higher plants.

This chapter summarizes the advances made in cryo-EM techniques and the structural data they have yielded for PS II and its antenna system with a particular focus on higher plants. Such studies are stepping-stones on the road to opening up the fascinating and dynamic 3D world of the in vivo chloroplast.

Abbreviations: 1D – one-dimensional; 2D – two-dimensional; 3D – three-dimensional; CCF – cross-correlation function; Chl – chlorophyll; CP43 – Chl *a*-containing protein with apparent molecular mass of 43kDa; CP47 – Chl *a*-containing protein with apparent molecular mass of 47kDa; Cryo-EM – electron cryo-microscopy; CTF – contrast transfer function; Cyt – cytochrome; Dpi – dots per square inch; EM – electron microscopy; FEG – field-emission gun; FSC – Fourier shell correlation; LHCII – light-harvesting complex of PS II; MSA – multivariate statistical analysis; NMR – nuclear magnetic resonance; OEC – oxygen-evolving complex; PCTF – phase contrast transfer function; PS II – Photosystem II; SNR – signal-to-noise ratio; TEM – transmission electron microscopy; TMH – transmembrane helix

II. Electron Cryo-Microscopy Techniques

Electron cryo-microscopy (cryo-EM) techniques involving the analysis of vitrified samples have revolutionized the structural analysis of macromolecular assemblies, allowing for medium resolution (7.5–30 Å) structures to be achieved from single particle images, and better than 5 Å from electron crystallography of 2D crystals. These techniques complement those structures visualized at lower resolutions by negative staining (Chen et al., 1998; Dubochet et al., 1988). The challenge of cryo-EM is to greatly increase the attainable resolution of the specimen under study, through careful preparation and imaging, in order to minimize electron-beam damage and maximize image contrast.

A. Specimen Preparation

Biological specimens are extremely sensitive to electron beam damage. Their atoms typically scatter electrons weakly, giving rise to low contrast (Chen et al., 1998) and high noise (Dubochet et al., 1988). In order to achieve higher contrast, negative staining techniques have been developed over considerable time, which are easy to implement, but impose some limitations. The main disadvantages are: (i) negative staining accentuates surface features at the expense of internal detail as the stain molecules do not penetrate past the surface of the protein. This imposes a resolution limit of 15–20 Å (Kiselev et al., 1990; Hoenger and Aebi, 1996). (ii) Stain artifacts can cause the variable flattening of the 3D structure by dehydration. Still, negative stain is valid for probing an unknown sample, often for initial 2D/3D structural impressions of the specimen, prior to images taken of vitrified samples that do contain information to atomic resolution. In the latter approach, with the samples embedded in vitreous ice, the molecules remain hydrated under conditions that resemble the native environment more closely.

B. High-Resolution Imaging

In order to produce high quality cryo-EM images using transmission electron microscopy (TEM) several requirements need to be fulfilled. The specimen stage, termed here a cryo-stage, must be mechanically stable, reducing drift during imaging and preventing the accumulation of electric charge, vibrations, stray magnetic fields and heat. The stage can be cooled by either liquid nitrogen or liquid helium (Dubochet et al., 1988; Fujiyoshi, 1998). The sample on the EM grid should be imaged under minimal electron dose conditions to reduce damage by the electron beam. Ideally, the region to be imaged consists of the biological sample embedded in a thin film of vitreous ice, which is suspended across a hole in the carbon foil. The sample is initially viewed at high magnification (150,000×), but on an area of carbon film slightly away from the ice hole, such that the electron beam is at a low dose and does not interact too harshly with the sample and cause irradiation damage – i.e., imaging is performed blind and the image quality only assessed after the film is developed. Phase contrast is then introduced by defocusing the microscope to ~1–2 μm underfocus. Exposures are typically made at ~50,000×, the beam only now interacting with the area to be imaged at high dose. The magnification at which the images are taken, accelerating voltage, total electron dose, and defocus can all be varied depending on the desired resolution. It should be noted that even the most advanced TEM optics are of poor quality in terms of astigmatism, spherical aberration, lens-current fluctuations and chromatic aberration, which can all be quantified in terms of the contrast transfer function (CTF) and corrected for to a certain extent. Another important development is that of the field-emission gun (FEG) (Stowell et al., 1998). A FEG-equipped EM uses very high electric fields to release electrons from a fine tungsten tip (Reimer, 1997). This increases the spatial and temporal coherence of the electron source, boosting the contrast transfer at high resolutions when compared to the standard thermionic emission gun.

Once TEM images of the highest quality are achieved, a range of analytical techniques can be applied depending upon whether the sample has been imaged for single particle analysis, electron crystallography or tomography.

C. Single Particle Analysis

Single particle analysis started developing after the demonstration that a 3D object imaged in an electron beam gave corresponding 2D projection images dependent on its orientation (DeRosier and Klug, 1968). If the angle for each of these 2D projections can be determined, a 3D structure of the molecule may be calculated by projecting the 2D images back along their projection angles, a technique known as back-projection (Radermacher, 1988). Electron

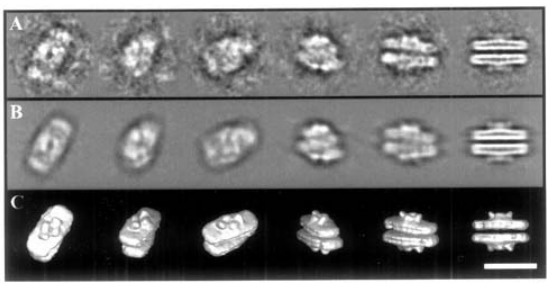

Fig. 1. 3D single particle analysis of the LHCII-PS II supercomplex (Nield et al., 2000c). (A) Selection of typical class averages used for the 3D reconstruction. (B) Reprojections of the 3D map in identical orientations with the corresponding class averages. (C) Surface representation of the final 3D map viewed in the same orientation as the class averages. Bar represents 30 nm.

micrographs of biological molecules are intrinsically noisy and exhibit low intrinsic contrast. Single particle averaging techniques significantly enhance the signal-to-noise ratio (SNR) present within the original images; in turn increasing the limits of resolution and interpretability (see Fig. 1). Now widely used for many structural biology-based problems, single particle averaging (or analysis), cryo- and negative stain-EM, have all recently been reviewed in depth (Orlova, 2000; Saibil, 2000a,b; van Heel et al., 2000; Ruprecht and Nield, 2001; Henderson, 2004). In this section we only briefly introduce the reader to the main steps involved.

1. Interactive Particle Selection and Band-Pass Filtering

First the electron micrographs are digitized by a high fidelity densitometer measured to be at least 2000 dpi, and are then corrected for the CTF (Reimer, 1997). A data set of at least several thousand particles is obtained from the micrographs by picking all discernible particles not overlapping or in close contact with other particles (Harauz et al., 1988). The single particle images are floated out into pixel boxes whose size is just enough to enclose the single particle images and remove as much background as possible. In order to suppress the extreme high and low spatial frequencies present within the images, certain band-pass filters can be applied. It is necessary to do this as very low spatial frequencies can cause fluctuations in the average density, for example the amount and uniformity of the staining, whereas in very high spatial frequencies the SNR is much smaller (Harauz et al., 1988). This can directly affect the success of the further alignment steps as the correlation functions used can emphasize certain spatial frequencies (van Heel et al., 1992). The spatial frequencies are only suppressed, so one can restore them after an initial 3D model has been reconstructed. This is especially important for the high spatial frequencies, which include desired high-resolution information.

2. Reference-Free Alignment and Multivariate Statistical Analysis

The first alignment step is reference-free alignment, which functions to center each particle within its pixel box through a series of translational shifts by using cross-correlation functions (CCFs) (Frank, 1980; Reimer, 1997). All processing is evaluated in Fourier space, taking advantage of the convolution theorem, which enables calculations to be processed many times faster in the computing environment. The reference-free alignment step is iterated several times until a good alignment is achieved while the data set is prevented from being biased towards any particular reference at an early stage in the analysis (Dube et al., 1993; Schatz et al., 1995). Multivariate statistical analysis (MSA), a form of correspondence analysis, is then used to identify the main components of variation within any given set of images, placing each image into a group of similar molecular images of similar rotational orientations. The mechanism of MSA reflects a form of data compression, greatly increasing the speed of the image processing, reducing the effects of noise, and may provide useful information about conformational flexibility or substrate binding (Saibil, 2000b).

3. Classification and Multi-Reference Alignment

In the Imagic-5 program suite, the hierarchical ascendant classification algorithm is used to generate a specified number of classes (van Heel and Stoffler-Meilicke, 1985). The algorithm starts with as many classes as there are images. It then merges the classes that are most similar, where if the resulting increase in total intra-class variance is minimal, each of these classes are then averaged to produce class averages (see Fig. 1A). These class averages have a higher SNR than the raw images and are more easily interpreted. Having produced initial class averages, some are used as references to search through and align the entire data set, generating improved class averages. In this multi-reference alignment (Schatz et al., 1995), each image is translationally and now also rotationally aligned using cross-correlation functions. After a number of iterative cycles much improved class averages are achieved.

4. Angular Reconstitution and 3D Reconstruction

Once improved class averages are achieved, the construction of a 3D model commences. The projection direction of each average, relative to the others, must first be understood (Euler angles). This assumes that all the 2D averages were imaged from identical 3D structures. Imagic-5 employs the angular reconstitution technique, based on the common line projection theorem (van Heel, 1987). An initial 3D reconstruction is calculated by back-projecting the class averages along their assigned Euler angles (Radermacher, 1988). The 3D reconstruction is then reprojected along the Euler angle directions assigned to the class averages (see Fig. 1B). This provides a means to compare how well their corresponding class averages fit to the 3D model (compare Fig. 1B with the class averages of Fig. 1A). Poor quality class averages, perhaps deriving from particles that became damaged prior to imaging (see heterogeneous populations section below), can be identified and removed from the dataset. The remaining class averages are then back-projected once more to produce a more reliable 3D model (see Fig. 1C). Refinement is possible by using the reprojected images from the latest 3D model as references in a new multi-reference alignment. After the 3D model shows no further improvement from iterative refinements, an estimation of the resolution is made by measuring the Fourier shell correlation (FSC) (Orlova et al., 1997; van Heel, 1986). Final presentation of the model is usually by surface-rendering the 3D map, or showing a series of its cross-sections, revealing internal density distribution.

Single particle analysis is able to deal with heterogeneous populations of molecules (van Heel et al., 2000; Ruprecht and Nield, 2001) and in the study of protein complexes that undergo conformational flexibility (Saibil, 2000b). MSA and classification allow a heterogeneous population to be sorted into classes of similar molecules, generating more homogeneous sub-populations for independent analysis, a form of 'computational purification.' This relatively novel application has been used in PS II studies to reveal different conformations of subunit binding (Nield et al., 2000a,c, 2002), and its use will increase as heterogeneous populations of molecules are very difficult to study by X-ray or electron crystallography. Indeed, use of this methodology has facilitated the study of PS II complexes in the recently discovered cyanobacterial organisms *Prochloron didemni* and *Prochlorococcus marinus*. This has revealed that a transmembrane light harvesting protein, Pcb, which is similar in structurre to CP43, binds to PS II reaction centers in a stochiometry of 5 or 4:1, respectively (Bibby et al., 2003a,b).

The best resolutions published to date using single particle analysis are 7.4 Å for the hepatitis B core protein (Böttcher et al., 1997) and 7.5 Å for the 70S ribosome (Matadeen et al., 1999), although 15–25 Å is more usual. Currently the resolution limit is imposed by factors including beam-damage, specimen movement, astigmatism, beam-induced specimen charging, aberrations, beam drift, and the inability to correct for the CTF perfectly. Assuming that image quality is not limiting in terms of the above parameters, an increase in the size of the single particle data set will increase the resolution of retrieved structural detail, suggesting that initially the low signal to noise ratio of cryo-electron micrographs is also a factor (Orlova, 2000). Typically, data sets of 20,000+ particles have proved necessary for the reconstruction of non-symmetric particles to intermediate resolution. In addition, it has been shown that one can exploit any molecular symmetry present to decrease the number of images needed for a given resolution (DeRosier and Klug, 1968; Chiu et al., 1999). Except for the computing power available, there is no upper limit to the size of molecule that can be studied by single-

particle analysis, a significant advantage compared to NMR spectroscopy, although a minimum size of 100 kDa has been suggested due to the requirements of molecular alignment (Henderson, 1995, 2004).

D. Electron Crystallography

In parallel with single particle analysis, electron cryo-crystallography has made rapid advances in recent years, to the point that it is now a viable alternative to X-ray crystallography, for high-resolution structure determination of membrane proteins. Indeed to date electron and X-ray crystallography are the only techniques, which have yielded structures of membrane proteins at, or approaching, atomic resolution.

Most membrane protein structures have been solved by the X-ray approach, although a large number of diverse membrane proteins are now at an advanced stage in their structure determination by electron crystallography. For example, the structure of bacteriorhodopsin has been solved with a resolution of 3.0 Å in the X-Y plane (Henderson et al., 1990; Mitsuoka et al., 1999) with those of LHCII (3.4 Å) (Kühlbrandt et al., 1994), aquaporin (3.8 Å) (Murata et al., 2000) and the cytoskeletal protein tubulin (3.7 Å) (Nogales et al., 1998). Furthermore as electron micrographs contain both amplitude and phase information, thus avoiding the phase problem of X-ray crystallography, a large number of important intermediate resolution structures such as those of the acetyl-choline receptor (4.6 Å) (Miyazawa et al., 1999, 2003), halorhodopsin (5.9 Å) (Kunji et al., 2000), Ca^{2+}-ATPase (6Å) (Xu et al., 2002), glutathione transferase (6 Å) (Schmidt-Krey et al., 2000), GlpF (6.9 Å) (Stahlberg et al., 2000), PS II (7–10 Å) and the NhaA Na^{+}/H^{+} antiporter (7.0 Å) (Williams, 2000) are being solved. These provide valuable information at the level of subunit, α-helix and, in some cases, β-sheet organization.

In contrast to X-ray crystallography, which requires well ordered 3D crystals for atomic resolution structure determination, electron cryo-crystallography requires high quality 2D crystals, which can be produced using either the bilayer or monolayer approach.

1. Bilayer Crystallization

Perhaps the simplest way of producing 2D crystals is by using the bilayer approach (Kühlbrandt, 1992; Hasler et al., 1998; Auer et al., 1999; Levy et al., 1999; Lebeau et al., 2001). Essentially 2D bilayer crystals are produced from purified and detergent-solubilized membrane proteins that are mixed with specifically selected lipids (Fig. 2A). This protein:lipid:detergent blend is depleted of detergent in a controlled manner (Fig. 2B-D) by dilution, dialysis or the addition of detergent-adsorbing beads (Bio Beads). During the initial stages of detergent removal 'rod-like' structures (Fig. 2B) are often observed (Hasler et al., 1998), and are thought to be part of the micelle-bilayer transition stage prior to crystal formation. In the case of PS II, further detergent depletion forces lipid:protein:detergent micelles to fuse along the second axis of the hydrophobic plane (Fig. 2C), giving protein-packed lipid bilayers and 2D crystal nuclei (Fig. 2C). These subsequently grow into 2D crystals (Fig. 2D).

2. Monolayer Crystallization

As its name suggests, this novel technique (Levy et al., 1999) uses a flat lipid monolayer as a template to produce 2D crystals of membrane proteins. The monolayer lipid mixture used is doped with functionalized lipids such as Ni-chelating or charged lipids for the crystallization of His-tagged or charged proteins, respectively. The method involves dispensing a monolayer-forming lipid mixture, dissolved in chloroform, on to the flat surface of a buffer droplet contained in a special crystallization well. Next, detergent solubilized His-tagged membrane proteins, supplemented with bilayer-forming lipids, are injected into the buffer below the monolayer via a side port. On incubation these His-tagged proteins bind to the Ni-chelating lipids in the monolayer. The 2D crystallization process is then induced by the addition of detergent-binding beads (Bio-Beads) via the injection port. As the proteins and bilayer-forming lipids are depleted of detergent, the membrane spanning regions of the membrane proteins begin to incorporate into a lipid bilayer. In the case of FhuA and F_0F_1-ATP synthase, 2D crystal patches were observed 1–2 days after detergent removal (Levy et al., 1999).

3. Electron Crystallographic Analysis

High quality 2D crystals are imaged in vitreous ice at tilt angles ranging between ± 70°, in angular tilt increments selected to attain the desired resolution. The negatives are then digitized using a precision scanner (see above) and the structural informa-

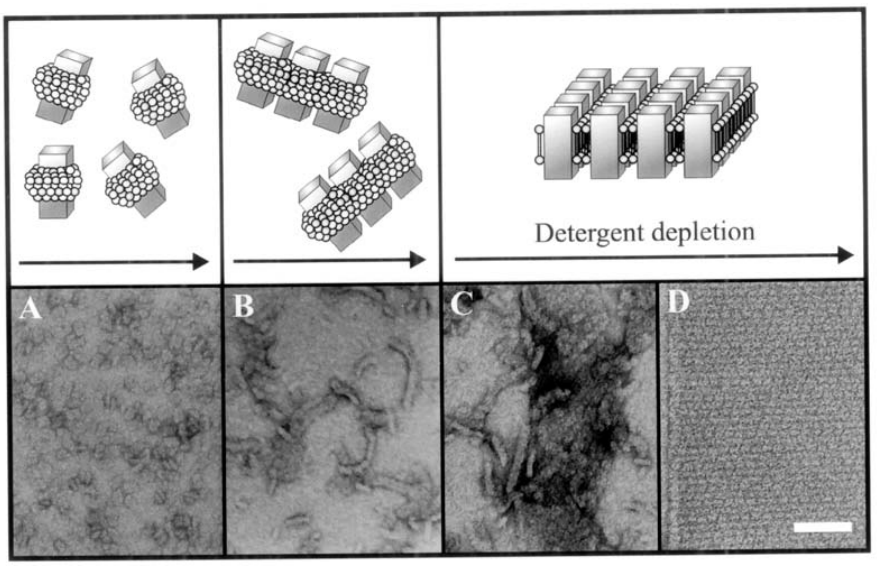

Fig. 2. The process of 2D crystal formation. Solubilized membrane proteins (A) aggregate into 'rod-like' structures (B), crystal nuclei (C) and finally form 2D crystals (D), the process captured by electron microscopy. Above is a diagrammatic version. Bar represents 100 nm.

tion contained in each tilt image is extracted using electron crystallographic approaches. These include filtering out noise unrelated to the crystal lattice and correcting for defects in the flatness and order of the crystal lattice itself (Henderson et al., 1986). The refined tilt images are then merged to generate a 3D reconstruction.

4. Advantages and Limitations of Electron Crystallography

Both the 2D monolayer and 2D bilayer approaches have the advantage over X-ray techniques given that the membrane protein of interest is embedded in a lipid bilayer in a near native environment. Under these conditions the membrane spanning domains of labile (non-rigid) membrane proteins are compressed through the lateral pressure of the lipid bilayer, aiding their stabilization. In theory, 2D crystals are also easier to grow as molecular arrangement is only required in two rather than three dimensions. In addition the electron micrographs of these crystals contain amplitude and phase information, thereby avoiding the lack of phase or 'phase problem' of X-ray crystallography, and allow structural information to be gained from small crystals and crystallization intermediates, the latter allowing for crystallization strategy development. The monolayer technique builds upon these advantages by favoring the formation of large flat bilayer sheet crystal types that are well suited for high-resolution studies. A number of factors can however limit the rate of high-resolution structure determination. Particularly important will be the development of streamlined approaches for high-resolution crystal production. In this respect the functionalized monolayer surface, used as a template in monolayer crystallization, has considerable potential. Other improvements that will benefit high-resolution electron crystallography are the use of new types of EM grids and support films that keep the 2D crystals as flat as possible (Vonck, 2000). The use of single particle techniques may also aid the recovery of high resolution data as the unit cells within a crystal can be classified prior to averaging rather than being subjected to global averaging (Sherman et al., 1998).

E. Electron Cryo-Tomography

In recent years great advances have been made in electron cryo-tomography allowing 3D reconstruction of individual organelles and whole cells to be deter-

mined using variations of the techniques employed for single particle analysis and electron crystallography (Baumeister et al., 1999). The adaptations being implemented address the issues of increased particle size (e.g., whole organelles vs. protein complexes) and the fact that individual organelles and cells do not have identical 3D structures, being fluid and dynamic in nature. Furthermore the technique has been developed to deal with specimens of ~0.25 to 2.0 μm thickness, by using TEMs capable of generating accelerating voltages greater than 400 kV (It should be noted that for single particle analysis or electron crystallography ~120–300 kV voltages are used). The word tomography itself defines that one freedom of rotation is fixed. In practice this means that the specimen being imaged is held in a fixed X-Y orientation while tilting the cryo-stage ± 70° in small increments e.g., 2°, in a manner similar to that employed for electron crystallography. As in the case of single particle analysis and given that these tilt angles are set by the user, back-projections of the tilt images can be made to generate a 3D reconstruction. Here the resolution-limiting factor is usually the precision with which such alignments can be made and the number of tilt images that can be taken of a single object before beam damage compromises the data.

Recent electron tomographic reconstructions have been made in the range 50–70 Å of mitochondria (Deng et al., 1999; Mannella et al., 1998; Perkins et al., 1997; Perkins et al., 1998) and a whole cell of the archaebacterium *Pyrodictium abyssi* (Baumeister et al., 1999). Recent improvements in the technique that have involved embedding the specimen in vitreous ice after plunging in liquid ethane, have aided the recovery of even higher resolution data, such as for *Neurospora* mitochondria (Nicastro et al., 2000). In addition, advanced single particle techniques for precise angular assignment and X-Y drift will help to improve resolution limits still further.

F. Summary

From the above, it can be seen that for a successful multi-disciplinary structural approach, X-ray and electron crystallographies and NMR spectroscopy would be chosen for studies involving individual molecules or small complexes, and single particle analysis employed for the study of larger complexes, present in different functional states or undergoing conformational flexibility. For organelles or whole cells, electron cryo-tomography can provide structural information at reasonably high-resolution. Subsequently, when available, previously determined smaller X-ray structures can be modeled into the larger single particle derived structural frameworks. Indeed this has been achieved over recent years in the field of PS II structural biology, extracting a wealth of new detail for the localization of the many light-harvesting components and co-factors that make up LHCII-PS II complexes, culminating in well-defined 3D structures containing over 50 subunits and having molecular mass in excess of a mega-Dalton.

In the following section we describe how this detail has emerged and how we might now start to use this information in understanding the multitude of in vivo processes that rely on such structure/function relationships.

III. Structure of Higher Plant Photosystem II and Its Antenna System

PS II is a multisubunit pigment-protein complex located within the thylakoid membrane of plants, algae and cyanobacteria and drives the highly oxidizing water splitting reaction. This reaction splits water into molecular oxygen, protons and electrons, thereby sustaining an aerobic atmosphere on Earth and providing the reducing equivalents required for carbon fixation on a global scale. The solar energy required to drive this highly oxidizing reaction is captured by specialized pigment-protein antenna systems, designed to transfer excitation energy efficiently to photochemically active reaction center (RC). Though similar in function, these antenna systems form a diverse range of structures, with those of higher plants and green algae being located in the thylakoid membrane, while those of most classes of cyanobacteria are bound extrinsically to the stromal surface of PS II. Cyanobacterial and higher plant PS II also differ in the lumenal extrinsic proteins associated with the oxygen-evolving complex (OEC) and in their complement of low molecular subunits. This section reviews the structural information obtained for the higher plant system, predominantly derived from single particle analysis and electron crystallography. To aid this process a brief review of PS II subunits is presented.

A. Subunits

1. The Core Complex

The PS II core complexes of higher plants, green algae and cyanobacteria all consist of over 20 subunits (Barber et al., 1997; Hankamer et al., 2001a; Barber, 2003). All of the redox active cofactors involved in the water photolysis reaction are bound to the reaction center proteins, D1 and D2 (Diner and Babcock, 1996; Chapter 4, Nixon et al.). Associated with these two proteins are the chlorophyll (Chl) *a*-binding inner-antenna proteins, CP43 and CP47 (Chapter 3, Eaton-Rye and Putnam-Evans), that have prominent lumenally-exposed protein loops, and the extrinsic lumenally bound proteins of the OEC (Chapter 5, Bricker and Burnap). The OEC provides an optimal micro-environment for the functioning of a four manganese atom cluster that catalyzes water oxidation. In higher plants and green algae, the OEC extrinsic proteins consist of the 33 kDa (PsbO), 23 kDa (PsbP) and 17 kDa (PsbQ) protein subunits, where PsbP and PsbQ are generally thought to be replaced by 9 kDa PsbU and 13 kDa PsbV (Cyt *c*550) proteins in cyanobacteria. In addition to PsbO, PsbP and PsbQ proteins, higher plants and green algae are reported to bind two other extrinsic proteins (PsbR and $PsbT_n$) on the lumenal surface (Barber et al., 1997). Over and above these subunits, the PS II core complexes of higher plants, green algae and cyanobacteria contain a large number of low molecular weight (LMW) intrinsic proteins (Table 1), including the α- and β-subunits of Cyt b_{559}.

Table1. Low molecular weight proteins of Photosystem II

Protein	Subunit	Mass (kDa)
PsbE (c)	α-Cyt b_{559}	9.255 (S)
PsbF (c)	β-Cyt b_{559}	4.409 (S)
PsbH (c)	H protein	7.697 (S)
PsbI (c)	I protein	4.195 (S)
PsbJ (c)	J protein	4.116 (S)
PsbK (c)	K protein	4.283 (S)
PsbL (c)	L protein	4.366 (S)
PsbM (c)	M protein	3.755 (P)
PsbN (c)	N protein	4.722 (T)
$PsbT_c$(c)	T_c protein	3.849 (S)
$PsbT_n$(n)	T_n protein	3.171 (A)
PsbW (n)	W protein	5.928 (S)
PsbX (n)	X protein	4.225 (S)
PsbY (n)	Y protein (A1)	4.673 (S)
PsbZ (c)	Z protein	6.541 (S)

These genes encode 15 low molecular mass PSII proteins of 10 kDa or less. The molecular masses of the mature proteins were calculated from the protein sequences reported in the SWISS-PROT data base using the MacBioSpec program (Sciex Corp., Thornhill, Ontario, Canada). The abbreviations given in brackets after the molecular masses denote the organism for which the subunit mass is given, as follows; *Arabidopsis* (A), pea (P), spinach (S) or tobacco (T).

2. The Antenna System

In higher plants the PS II core complex is linked to an outer antenna system (Fig. 3A) (Chapter 2, Green and Gantt) consisting of six different, but related, membrane proteins (Lhcb1-6) (Green and Durnford, 1996) all of which bind Chl *a*, Chl *b* and carotenoids (Liu et al., 2004). Similar Chl *a*/*b*-binding proteins also make up the outer antennae of green algae, although the number of different types is often larger, e.g., as in *Chlamydomonas*. The structures of two of the higher plant proteins, Lhcb1 and 2, which form a heterotrimer, were determined at a resolution of 3.4 Å by electron crystallography (Kühlbrandt et al., 1994). Each monomer was found to have three transmembrane helices and one surface helix. Seven Chl *a*, six Chl *b* and two carotenoid molecules were also identified in each monomer. Based on this structural information and the sequence homology between the six Lhcb proteins the remaining four are also predicted to have three transmembrane helices and to ligate pigments in a similar way. Another PS II protein, PsbS shares considerable homology with the Lhcb proteins, except that it is predicted to have four transmembrane helices (Green and Durnford, 1996). In the case of cyanobacteria a soluble, extrinsic, phycobilisome antenna system dwarfs the PS II core dimer in size and binds to it on the stromal side, one allophycocyanin core subunit binding to the dimer of the complex (Fig. 3B). The allophycocyanin core (ALC) usually, but not always, consists of three rods lying across the surface of the membrane. From the ALC, rods of phycocyanin radiate out, although in red algae, which also have phycobilisomes, other phycobilins such as phycoerythrin are present. Information on the structure of these water-soluble phycobiliproteins has been derived by X-ray crystallography (Brejc et al., 1995; Adir et al., 2001; Nield et al., 2003) while EM has contributed to our understanding of how

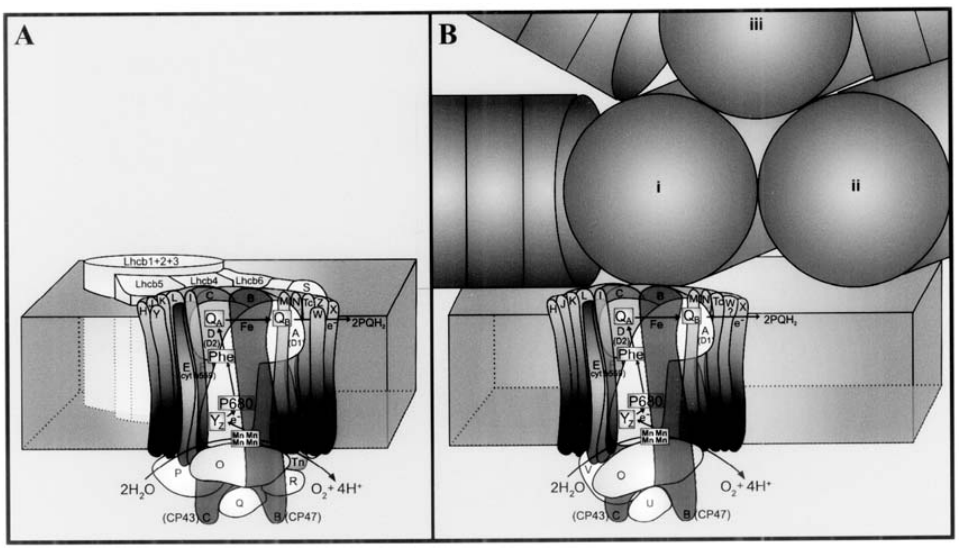

Fig. 3. Cartoons of PS II and its associated light-harvesting components (A) of higher plants and green algae and (B) of cyanobacteria, emphasizing subunit composition and primary and secondary electron transfer steps that occur in the reaction center D1 and D2 proteins. In the case of the higher plants and green algae (A) note that the secondary antenna is made up of Chl *a/b* binding Lhcb proteins, intrinsic to the membrane, while in (B), the cyanobacterial PS II is serviced by a large extrinsic, soluble phycobiliprotein mass on its stromal side. Also note, when comparing the two systems, the compositional differences present for the lumenally bound extrinsic subunits of the OEC. See Color Plate 3, Fig. 1.

they associate to form phycobiliproteins (Morschel and Schatz, 1987; Ducret et al., 1998; da Fonseca et al., 2002).

B. The Core Dimer Structure

Most of the structural details of the higher plant PS II core complex have been determined by electron crystallography, although 3D crystals have been reported (Fotinou et al., 1993; Adir, 1999). However, X-ray structures of a cyanobacterial PS II core complex have now been published (Zouni et al., 2001; Kamiya and Shen, 2003; Ferreira et al., 2004) that allow for comparisons with the higher plant complex to be made. For spinach, two distinct PS II preparations have been isolated that have yielded 2D crystals. The first is a monomeric RC-CP47 subcomplex (dark grey region Fig. 5) (Rhee et al., 1997, 1998), the second an oxygen evolving core complex (Morris et al., 1997; Hankamer et al., 1999, 2001b). The oxygen evolving PS II core complex is a dimer with each monomer component consisting of the D1 and D2 reaction center (RC) subunits, the inner antenna Chl binding proteins, CP47, CP43 and the extrinsic 33 kDa proteins, as well as a number of small membrane proteins, including the α- and β-subunits of Cyt b_{559} (Hankamer et al., 1997b). Electron microscope images of such crystals have yielded a 3D map in negative stain (Morris et al., 1997), a cryo-projection map (Hankamer et al., 1999) and later a 3D structure at a resolution of 10 Å resolution parallel to the membrane plane, again using vitrified samples of non-stained crystals (Hankamer et al., 2001b).

1. The Major Polypeptide Subunits

The side view of the 3D map (Fig. 4A and Fig. 1A of Color Plate 4) of the PS II spinach core dimer (Hankamer et al., 2001b) emphasizes the transmembrane region of the complex (containing fitted helices) and the extensive protrusion of density from the lumenal surface. The two large lumenal domains are thought to correspond to the location of the large lumenal loops of CP43 and CP47 (Fig. 4B and Fig. 1B of Color Plate 4). The positions of the transmembrane helices of the intrinsic PS II subunits (Fig. 4C and Fig. 1C of Color Plate 4) are derived from consideration of the distribution of density within the membrane

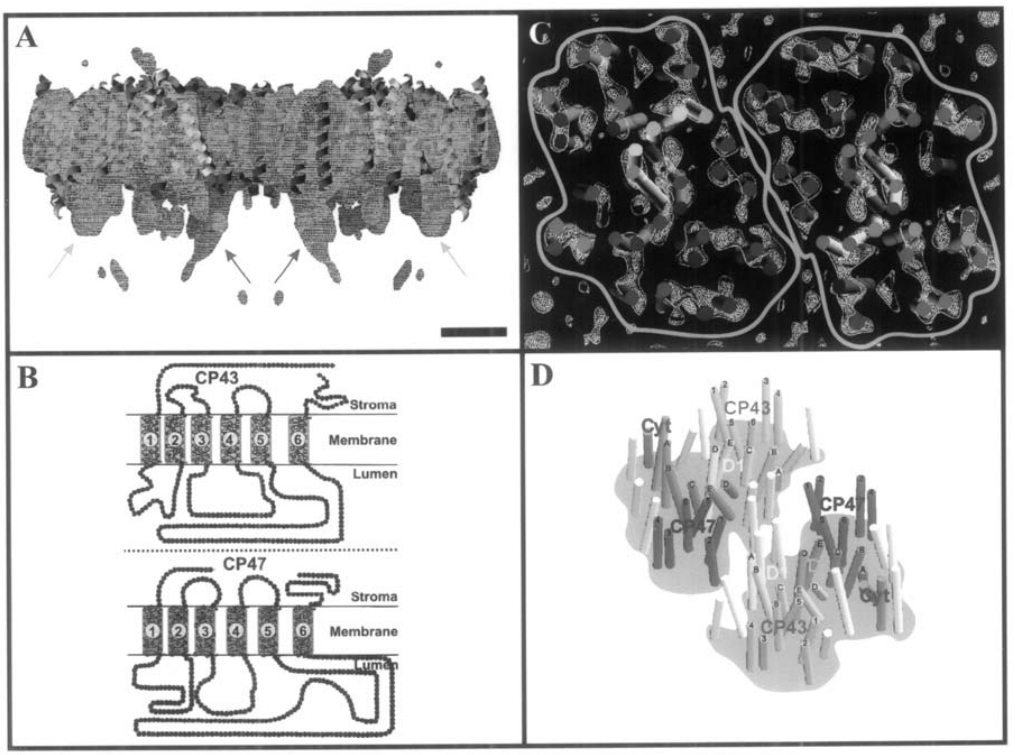

Fig. 4. (A) Side view of the 3D map of the spinach PS II core dimer, stromal side uppermost, emphasizing the transmembrane region and lumenal extensions assigned to the loops joining helices 5 and 6 of CP47 (innermost arrows) and CP43 (outermost arrows) (Hankamer et al., 2001b). (B) Predicted folding from hydropathy analyses of CP43 and CP47 (Hankamer et al., 2001b). (C) Transmembrane view of a section of the 3D map of the spinach PS II core dimer (Hankamer et al., 2001b). The map is sampled at ~1 Å and is displayed as chicken-wire contours, with compensation for high-resolution fade out (outer black contours, temperature factor –1000, 1.5 σ) and with no compensation (inner white contours, 1.3 σ). (D) An oblique view of the 3D structural model of the spinach PS II core dimer from electron crystallography. Bar for panels A and C represents 2.5 nm. See Color Plate 4, Fig. 1.

region. In each case the densities correspond either to individual or pairs of transmembrane helices that can be traced through the membrane plane. The assignment of helices to particular subunits relies in part on comparison with earlier electron crystallographic data obtained from the spinach PS II subcomplex containing the D1/D2 proteins and CP47 (Rhee et al., 1998). Thus the five yellow and five orange transmembrane helices within each monomer have been assigned to the D1 and D2 proteins, respectively. As noted previously their arrangement around a local pseudo-2D fold axis is remarkably similar to that of the L and M subunits of the reaction center of purple bacteria (Deisenhofer et al., 1984). All the transmembrane helices of the D1/D2 heterodimer are accommodated within the density of the map when no compensation is made for high resolution fade out at a threshold of 1.3 σ (blue contours). The positions of the transmembrane helices are better resolved when the high-resolution components of the data are accentuated using a threshold of 1.5 σ (white contours). The six helices colored red, adjacent to the D2 proteins and close to the monomer-monomer interface, belong to CP47. Additional density within the six helical cluster can be attributed to Chl molecules previously identified within the CP47 domain (Rhee et al., 1998). An equivalent set of densities was found adjacent to the D1 protein, and is related to those of the transmembrane helices of CP47 by the local two-fold pseudo-axis of the D1/D2 heterodimer.

These densities accommodate three pairs of helices assigned to CP43 (colored green). As in the case of CP47, additional density within the rings of helices is assumed to be due to bound Chl molecules. The assignment of the CP43 transmembrane helices was suggested previously based on a 2D projection map (Hankamer et al., 1999), but this is now supported by the 3D map in which the densities can be traced across the membrane. Two additional helices, colored cyan, are attributed to the α- and β-subunits of Cyt b_{559} (Rhee, 2001; Zouni et al., 2001; Kamiya and Shen, 2003; Kargul et al., 2003; Ferreira et al., 2004). The remaining transmembrane helices, colored in magenta, belong to the LMW subunits of PS II and will be discussed below.

The numbering of the helices of the D1 and D2 proteins in Fig. 4D and Fig. 1D of Color Plate 4 is based on a direct comparison with the structures of the L and M subunits of purple bacterial reaction center, with which they have a high degree of homology. The numbering of the six transmembrane helices of the CP43 and CP47 is based on structural analogies with the 6 amino-terminal (N-terminal) transmembrane helices of the Photosystem I (PS I) reaction center proteins PsaA and PsaB (Jordan et al., 2001). As shown in Color Plate 4, Fig. 1B, transmembrane helices 5 and 6 of CP43 and CP47 are linked by large lumenal loops consisting of 150 and 200 amino acid residues, respectively. In Color Plate 4, Fig. 1A, green and red arrows are used to indicate significant density protruding from the lumenal surface. Based on the helix assignment shown, it was concluded from the surface topography of the map that these lumenal protrusions are located above the helix pairs assigned to 5 and 6 of CP43 (in green) and CP47 (in red). This conclusion is therefore consistent with the existence of the large loops and the assignment of helices 5 and 6 of CP43 and CP47 in our structural model.

2. Extrinsic Lumenal Proteins

Closely associated with the PS II reaction center D1, D2, CP47 and CP43 proteins are the extrinsic lumenally bound proteins of the OEC. As mentioned above, the OEC extrinsic proteins consist of PsbO, PsbP and PsbQ proteins in higher plants and green algae, with PsbP and PsbQ being replaced by PsbU and PsbV in cyanobacteria. Two other minor extrinsic proteins have also been identified as being bound on the lumenal surface, PsbR and $PsbT_n$ (Barber et al., 1997; Barber, 2003), whose function is as yet unknown. The PsbO protein has generally been accepted as holding a major role in optimizing OEC function and thus water oxidation. In the EM-derived 3D map of Hankamer et al. (2001b), insufficient density was found to accommodate the PsbO protein despite evidence from SDS-PAGE gels that this protein was present in the samples used for electron microscopy (Hankamer et al., 1999). However, studies using single particle analysis, cryo-EM and various biochemical treatments to sequentially wash off the extrinsic proteins, have revealed significant density protruding into the lumen. These 3D difference cryo-EM maps, resolved in the 17–26 Å range, for higher plant LHCII-PS II supercomplexes (Nield et al., 2002) were interpreted as containing one copy of the PsbO per reaction center. Another 2D study involving negatively stained top views supported this as the most likely outcome (Boekema et al., 2000b). Both studies were able to relate the positions of the 33 kDa protein to the underlying intrinsic membrane proteins through 3D and 2D modeling studies, respectively. The more recent X-ray derived maps at 3.5 to 3.8 Å resolution (Zouni et al., 2001; Kamiya and Shen, 2003; Ferreira et al., 2004) also support one PsbO per reaction center in cyanobacterial systems. Investigations into the positional relationships between PsbO and PsbP / PsbQ, or PsbU/PsbV in cyanobacteria, will undoubtedly provide intriguing insights into the evolutionary development of the OEC and the mechanisms necessary for efficient water oxidation (De Las Rivas et al., 2004).

3. The Minor Polypeptide Subunits

In addition to the 22 helices of the major subunits a further 12 transmembrane helices assigned to low molecular weight subunits were identified in the PS II core dimer map (Hankamer et al., 2001a,b). For clarity these have been numbered from i-xii in Fig. 5 and compared with those present in the previously determined CP47-RC subcomplex (Rhee et al., 1998). The helices identified in the CP47-RC subcomplex map are contained in the dark blue region regions shown in Fig. 5A ;and Fig. 2A of Color Plate 3.

It should be noted that the two helices previously assigned immediately adjacent to the B-helices of the D1 and D2 proteins in the map of CP47-RC subcomplex (Rhee et al., 1998), have not been included. It is highly likely that the densities in these regions are due to Chl molecules ligated to D1-His198 and D2-His198 rather than to transmembrane helices

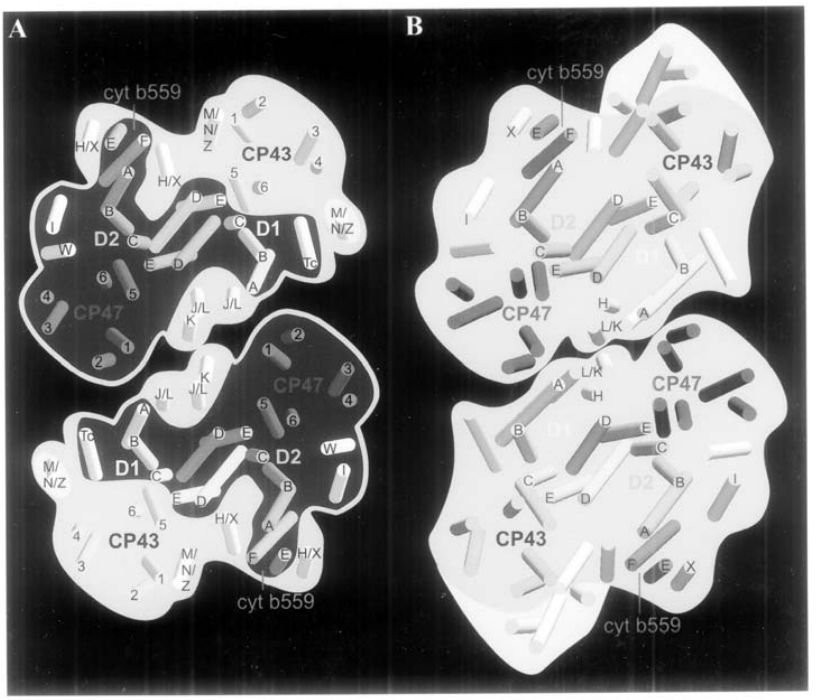

Fig. 5. Comparison of the PS II core dimer of (A) spinach (Hankamer et al., 2001b) and (B) *S. elongatus* (Zouni et al., 2001), and respective assignments of the low-molecular weight single transmembrane helical subunits. The dark grey region in (A) shows the helix organization of the spinach CP47-RC subcomplex (Rhee et al., 1998), which had to be modified, two transmembrane helices adjacent to helix B of the D1 and D2 proteins being removed. The remaining light grey regions contain the additional transmembrane helices of CP43 and other low-molecular weight core dimer subunits. See Color Plate 3, Fig. 2**.**

(Hankamer et al., 2001b). The revised number of LMW subunits in the CP47-RC subcomplex is consistent with mass spectrometry data and N-terminal sequencing analyses of an isolated and monomeric form of this CP47-RC subcomplex, which identified the five LMW proteins; PsbE, PsbF, PsbI, $PsbT_c$ and PsbW (Zheleva et al., 1998).

PsbE and PsbF, the α- and β-subunits of Cyt b_{559}, respectively, have been unambiguously identified in cyanobacterial X-ray structures (Ferreira et al., 2004). Based on their location in the cyanobacterial structures and on previous studies (Rhee, 2001), the two purple helices (Color Plate 3, Fig. 2A) were assigned to PsbE and PsbF as shown. With two of the five LMW protein helices of the CP47-RC subcomplex accounted for, the three remaining LMW proteins, PsbI, $PsbT_c$ and PsbW, can be attributed to the gray helices in the dark blue domain of Color Plate 3, Fig. 2A. The PsbI protein has been shown to cross-link both with the D2 protein and Cyt b_{559}, suggesting that it is on the D2 rather than the D1 side of the reaction center (Tomo et al., 1993). Furthermore, the PsbI protein is tightly associated with the isolated D1/D2 heterodimer while PsbW and $PsbT_c$ are less so (Irrgang et al., 1995; Webber et al., 1989). Consequently we tentatively assigned PsbI to the gray helix, closest to the D2 protein and Cyt b_{559}. Based on this assignment and on the report that PsbW can also be cross-linked to the α-subunit of Cyt b_{559} (PsbE) (Büchel et al., 2001) as well as co-purifying with the D1/D2/Cyt b_{559} RC complex (Irrgang et al., 1995), the second gray helix on the D2 side has been tentatively designated as PsbW. By elimination, $PsbT_c$ can therefore be assigned to the last gray helix in the CP47-RC subcomplex located adjacent to helices A and B of the D1 protein (see Color Plate 3, Fig. 2A).

In addition to the five LMW proteins within the

CP47-RC subcomplex, seven other LMW proteins have been attributed to membrane spanning densities identified in the higher plant PS II core dimer (Color Plate 4, Fig. 1). These additional LMW proteins are indicated as gray rods within the cyan domain of Color Plate 3, Fig. 2A. Of these seven proteins, four have been identified in our spinach dimer core complex by N-terminal sequencing and mass spectrometry; PsbH, PsbL, PsbK, and PsbX. PsbL and PsbK were also previously found in a dimeric, but not monomeric, forms of the spinach CP47 RC complex (Zheleva et al., 1998). This suggests that PsbL and PsbK are likely to be located in the central cyan regions at the interface between the two CP47-RC subcomplexes within the dimeric structure (Color Plate 4, Fig. 1). They may therefore account for two of the three transmembrane helices in this central linker region. In this context it is interesting to note that the pseudo-two-fold symmetry axis which relates the D1 and D2 proteins as well as CP47 and CP43, also approximately relates PsbE and PsbF with two of the gray helices in this central domain found adjacent to helix A of the D1 protein. Furthermore, in most organisms the PsbE, PsbF, PsbJ and PsbL are all coded for by a single chloroplast operon and expressed on a tetracistronic message. This suggests the intriguing possibility that the helix pair roughly symmetrically related to PsbE and PsbF consists of PsbJ and PsbL. Also as noted in Table 1, PsbJ and PsbL have highly conserved amino acid sequences. Consequently these two helices have been labeled J/L placing PsbK closest to the contact point of the PS II core dimer (Color Plate 3, Fig. 2A).

The two remaining LMW proteins that have been identified in the higher plant PS II core dimer are PsbH and PsbX. Recently the PsbH protein was shown to cross-link with the PsbE subunit of Cyt b_{559} in PS II core dimers isolated from the green alga *C. reinhardtii* (Büchel et al., 2001). Using a combination of gold labeling and single particle analysis, it was confirmed that the PsbH subunit was localized to a position close to Cyt b_{559}. As the PsbX subunit has been shown to be cross-linked with PsbH (Büchel et al., 2001) as well as with PsbE (Shi et al., 1999; Büchel et al., 2001) it is suggested that the two helices close to PsbE and PsbF are either PsbX or PsbH. This leaves two unassigned transmembrane helices in the cyan regions of the PS II core dimer. The first of these is adjacent to the helix that we have assigned to $PsbT_c$, with the second located close to helices 1 and 2 of CP43. The remaining three possible gene products that have been suggested to be part of the hydrophobic core of the PS II complex are PsbM, PsbN and PsbZ. Indeed, there is evidence that PsbZ is located close to CP43 (Swiatek et al., 2001). Therefore these helices have tentatively been assigned to M, N or Z as shown in Color Plate 3, Fig. 2A. In cyanobacteria, a cluster of transmembrane helices is observed adjacent to CP43 (Zouni et al., 2001; Kamiya and Shen, 2003; Ferreria et al., 2004), which are absent in the spinach dimer. These may function to link the phycobilisome antenna system of the cyanobacterium to the PS II core dimer. Another possibility is that they confer thermostability, demonstrated by *S. elongatus* PS II being able to grow at 70 °C.

It should be noted that in light of the recent, more highly resolved X-ray structure of Ferreira et al (2004), comparisons regarding the assignment and possible functions of LMW proteins in higher plands need to be rerconsidered (Chapter 21, Barber and Iwata).

C. Evolutionary Implications

The higher plant and cyanobacterial PS II core complexes are both dimeric and the organization of the transmembrane helices of the major subunits, D1, D2, CP43 and CP47 are very similar (Color Plate 3, Fig. 2). The existence of such conserved features amongst these species reinforces the view that the PS II of higher plants and cyanobacteria have a common evolutionary origin. A comparison of the two structures also provides strong evidence that the dimeric nature of the core is the main physiological form of PS II both of higher plants and cyanobacteria. The similarities of the two structures are also carried through to the level of the LMW subunits. The position of Cyt b_{559} and two adjacent small subunits appear to be conserved, as are the cluster of three helices (J, K and L) at the interface between the two monomers (Color Plate 3, Fig. 2A). Transmembrane helices denoted I, Tc and W are also found in both structures. The differences are that in cyanobacterial PS II, a helix putatively assigned as M/N does not appear to be present, but instead an additional cluster of three helices exists, sitting between Cyt b_{559} and helices 1 and 2 of CP43, where only one helix was identified in the higher plant complex. It is possible that these differences relate to the intrinsic versus extrinsic nature of the light-harvesting systems of the two types of photosynthetic organisms, which we discuss below.

D. The Outer Antenna System

A variety of LHCII-PS II complexes exist, whose function is to form an excitonically coupled pigment network in order to capture light energy and transfer it to the PS II RC (Boekema et al., 1995, 1999b). In higher plants the first such high-order complex to be isolated was a LHCII-PS II supercomplex from spinach (Hankamer et al., 1997b) and a similar complex was subsequently purified from the green alga *Chlamydomonas reinhardtii* (Nield et al., 2000b). Both structures were determined at intermediate resolution by single particle analysis and showed considerable homology (Nield et al., 2000b,c), measuring ~330 × 165 × 110 Å. LHCII-PS II super- and mega- complexes isolated from liverwort (*Marchantia polymorpha*) were also structurally similar (Harrer, 2003). The PS II oxygen-evolving core dimer forms the central region of the supercomplex, flanked by two clusters of the Chl *a*/*b* binding subunits Lhcb1, 2, 4, 5 (Hankamer et al., 1997b; Nield et al., 2000c). Each cluster was found to be composed of a LHCII trimer (Lhcb1 and 2) at its outermost tip, which appears to be structurally and excitonically coupled to the PS II core dimer via Lhcb proteins 4 and 5 monomers, also known as CP29 and CP26, respectively. Lhcb4 and 5, together with another Lhcb component, Lhcb6 (sometimes known as CP24), are thought to facilitate the binding of additional LHCII trimers, probably containing Lhcb3 as well as Lhcb1 and Lhcb2, to the edge of the supercomplex, leading to the possibility of still higher order structures being formed (Boekema et al., 2000a).

To further investigate subunit positioning, the transmembrane helical organization of the higher plant core dimer derived from electron crystallography has been modeled into a 17 Å 3D map of the spinach LHCII-PS II supercomplex obtained by single particle analysis (Nield et al., 2000a). This reconstruction also included the Lhcb components, which can be modeled as helices based on the electron crystallographic structure of LHCII (Kühlbrandt et al., 1994). The modeling revealed such details as two LMW membrane proteins, adjacent to helix B of the D1 protein, and appearing to form a link to the LHCII trimer. To be noted is that in cyanobacteria one of these helices is not present (see Color Plate 3, Fig. 2). In this case, the inference has been that over and above a purely structural role it is possible that this additional LMW subunit mediates excitation energy transfer from the outer light-harvesting antenna directly to the reaction center.

Boekema et al. (1999a,b) have performed several studies attempting to search for complexes larger than that currently defined as the LHCII-PS II supercomplex. Their approach has been to subject PS II membranes to partial detergent treatment, analyzing the solubilized membrane patches by single particle analysis, and computationally purifying the dataset. This has shown that LHCII can bind in three ways, strong (S), moderate (M) and loose (L) in three different forms of PS II 'megacomplex'. More recent work has classified images of crystalline arrays of PS II from spinach granal membranes, indicating that crystalline regions contain predominantly LHCII-PS II supercomplexes, and that the megacomplexes may be relegated to non-crystalline areas (Boekema et al., 2000a). As mentioned above, PsbS, shares considerable homology with the Lhcb proteins, except that it is predicted to have four transmembrane helices (Green and Durnford, 1996), and it is likely to be present in these larger, megacomplexes since it is not present in the isolated LHCII-PS II supercomplex (Nield et al., 2000a). The most significant conclusion from all this work is the heterogeneous nature of the associations between PS II and LHCII. It has been proposed that the formation of these different complexes may allow PS II to react to light and stress conditions by providing different routes of excitation energy transfer (Boekema et al., 1999b).

The typical inherent heterogeneity of higher plant/green algal systems does add another dimension of difficulty for structural studies, which has been overcome to a certain degree by 'computer purification' single particle analysis methods, as in relating the position of the OEC extrinsic proteins (Nield et al., 2002). These have shown that by classifying PS II complexes on the amount of peripheral proteins they contain, deductions about how the subunits fit together can be made, and this is also likely to prove a valuable methodology for structural investigations into photosystem and light-harvesting dynamics.

IV. Organization and Dynamics of Higher Plant Photosystem II and Its Antenna In Vivo

The thylakoids of higher plants (Fig. 6A) and to a lesser extent, green algae (Fig. 6B), form intricately arranged 3D membrane networks, segregated into stacked granal and unstacked stromal lamellae. This is

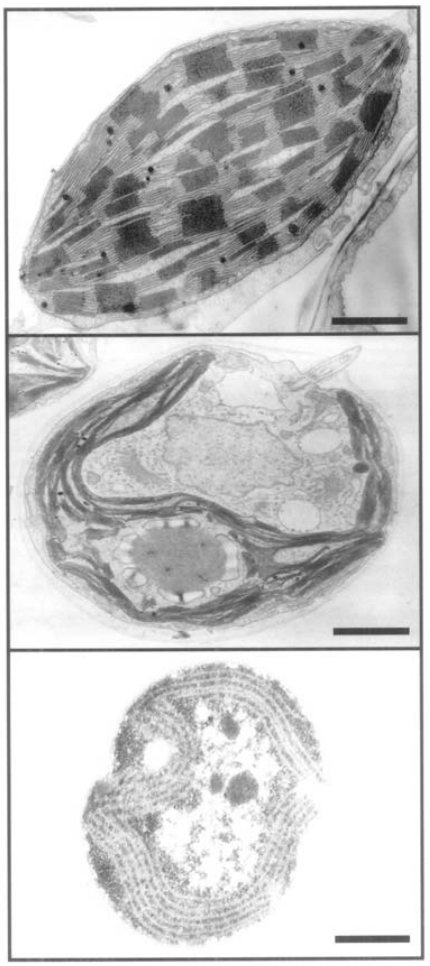

Fig. 6. Typical cross-sections of thylakoid membranes from (A) higher plants, bar represents 1 μm, (B) green algae, bar represents 10 μm, and (C) cyanobacteria, bar represents 10 μm.

in contrast to most cyanobacteria in which the membranes are unstacked (Fig. 6C). It is widely reported that PS II, PS I and ATP synthase in higher plants are spatially separated within these two compartments. PSI and ATP synthase are predominately located in the stroma lamellae while active PS II is present in abundance within the grana (Andersson and Anderson, 1980; Barber, 1980, 1982), with Cyt $b_{6}f$ complex found in both (Albertsson, 1995). However this is a rather static picture of a highly dynamic membrane system. During chloroplast maturation, for example, extensive cubic phase lipid membrane networks observed in etioplasts are converted to the intricate lamellar membrane systems of the grana and stroma lamellae. This process is accompanied by protein synthesis, insertion and segregation to arrive at the mature protein distributions described above. Even in the mature system specific outer light-harvesting antenna Lhcb proteins shuttle between PS II in the grana and PS I in the stroma to optimize electron transport through the two photosystems (Kruse, 2001). Furthermore, the D1 exchange process is reported to involve extensive migration of damaged and repaired CP47-RC subcomplexes between the grana and the stroma lamellae (Zhang and Aro, 2002; Barbato et al., 1992). To develop a picture of the dynamics of PS II and its antenna system in vivo, this section focuses on EM studies of PS II and its antenna system within the native thylakoid membrane.

A. Freeze-Etch and Freeze-Fracture Techniques

Freeze-etch and freeze-fracture microscopy are well suited for imaging the surfaces of membranes and their embedded components. In the freeze-etch process, excess surface water is evaporated from flash frozen membranes under vacuum (typically –100 °C), to reveal the surface contours of the embedded membrane proteins. Subsequent platinum shadowing can further enhance visualization. In contrast, the freeze-fracture process is used to study the structure of membrane embedded components of native membranes. To achieve this, flash frozen thylakoid membranes are cleaved along the internal hydrophobic plane of a bilayer prior to imaging. In such a manner, the thylakoid membrane ultrastructure has been studied extensively for a large number of organisms, including barley, spinach, maize, lettuce, soy bean, *Portulaca*, *Alocasia* and pea (Hankamer et al., 1997a).

A number of reviews in the literature have remarked upon similarities in membrane protein distribution (Miller, 1981; Albertsson, 1995; Hankamer et al., 1997a). In each case a range of membrane protein complexes differing in size and shape were detected and named according to the surfaces in which they were located, as defined by freeze-etch terminology developed by Staehelin (Staehelin, 1976, 1986). Here ESs, PSs, ESu or PSu refer to the endoplasmic (E) and protoplasmic (P) surfaces (S) of stacked (s) and unstacked (u) freeze-etched thylakoid membranes. The corresponding freeze-fracture (F) planes are

referred to as EFs, PFs, EFu and PFu. The constituent components of these particles were in many cases identified by the analysis of mutant membranes. For example, comparison of PSI deficient mutant thylakoid membranes showed that this photosystem formed part of the large PFu particles. Localization of complexes in the stacked and unstacked thylakoid membranes was further facilitated by antibody labeling (Olive and Vallon, 1991).

B. Localization in the Thylakoid Membrane

Through the use of freeze-etch and freeze-fracture techniques, comparative studies of wild type and PS II deficient mutants of tobacco have shown that the thylakoid membranes of the latter to be depleted of ESs and EFs particles, normally located in the grana (Miller and Cushman, 1978). From these results it was concluded that such ESs/EFs particles correspond to the extrinsic and internal parts of PS II respectively. Support for this conclusion came from parallel studies of PS II deficient barley mutants (*xantha*-b12, *viridis*-c12, *viridis*-e64 and *viridis*-zd69), whose granal membranes were also greatly depleted of EFs particles (Simpson, 1978; Staehelin, 1986). The antenna proteins were located using Lhcb protein deficient mutants (e.g. barley mutants *xantha*-l35 and *viridis*-k23 and *chlorina*-f2) and by comparing thylakoid membranes from light and dark grown plants, the latter being depleted in these antenna proteins (Miller et al., 1976; Armond and Arntzen, 1977; Simpson et al., 1978; Simpson, 1979). Freeze-etch images of Lhcb protein depleted membranes also showed the ESs particles to be smaller. Together these results suggested that the PFs particles contained the Lhcb antenna proteins and that they were closely associated with PS II (EFs and ESs) particles in native membranes.

The close association of PS II and Lhcb proteins was characterized in more detail by the analysis of 2D crystalline arrays of ESs complexes (Miller, 1981; Seibert et al., 1987; Simpson, 1979). An image of such an array (Fig. 7) shows a section of the freeze-etch surface (ESs surface) and a part of the protoplasmic fracture face (PFs surface). The Lhcb proteins (PFs particles in the PFs fracture face) have been shown to fit in register into the grooves between the PS II complexes (ESs particles in the freeze-etched ESs surface) thereby providing strong evidence for the existence of supercomplexes of PS II and its light-harvesting antenna system (Hankamer et al., 1997b).

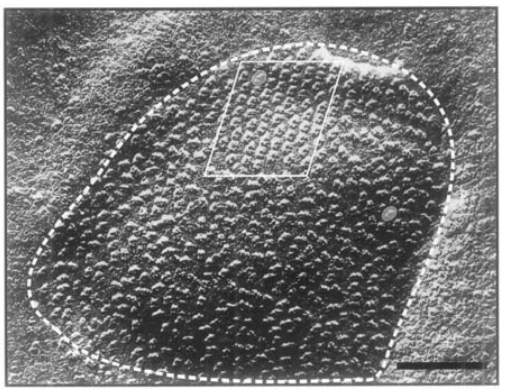

Fig. 7. A lumenal surface of stacked spinach thylakoids revealed by freeze-etching, delineated by a white dashed line, showing the ESs particles attributed to PS II (Seibert et al., 1987). Prior to freeze-etching, the preparation was biochemically washed to remove the OEC extrinsic proteins, which revealed each particle, typically 20 nm in length, to have underlying dimeric features as emphasized here by 2 gray circles. A native 2D array is also shown within a solid white line. Bar represents 100 nm.

C. Heterogeneity—2D Arrays and Randomly Oriented Supercomplexes

The ESs and EFs particles, which contain PS II, are not evenly distributed within the thylakoid membrane. Freeze-etch and freeze-fracture studies have shown that ESs and EFs particles respectively, can be organized into 2D arrays (see Fig. 7) or be more randomly dispersed within the grana. PS II-like particles are also observed in the stroma lamellae. It has been calculated that 85% of PS II particles are located in the granal stacks, which are often referred to as PS IIα. The remaining 15% of PS II complexes are located in the stroma and are termed PS IIβ (Albertsson, 1995; Andersson and Anderson, 1980). PS IIα complexes have approximately twice the antenna size of the PS IIβ complexes (Anderson and Melis, 1983) and are more efficient at reducing ferricyanide and duroquinone (Henrysson and Sundby, 1990). The PS IIα complexes are also more abundant and active than PS IIβ and have yielded most of the available structural data.

The PS IIα population in the grana can itself be divided into subpopulations of differing antenna size (Albertsson et al., 1990) which is consistent with the recent work of Boekema and colleagues (Boekema et al., 1999a,b). Interestingly, freeze-etch studies have shown that some ESs particles within the grana form

2D arrays, while others are more randomly dispersed, forming at least two sub-populations (Simpson, 1979; Seibert et al., 1987). Several publications provide the dimensions of arrayed ESs particles. Wild type ESs arrays in barley are reported to have unit cell dimensions of 175 × 247 Å, 180 × 225 Å and 180 × 240 Å (Seibert et al., 1987), while those of desaturase mutants of *Arabidopsis thaliana* are 190 × 230 Å and 180 × 230 Å (Tsvetkova et al., 1995). More recently, (Boekema et al., 2000a) identified two different lattice types in ordered 2D arrays of LHCII-PS II complexes isolated from spinach thylakoids by mild detergent solubilization. Two types of arrays appeared to reflect the in vivo organization of PS II and its antenna. These were identified to have row spacings of 263 Å and 230 Å respectively. The small-spaced crystals were reported to be less common but more highly ordered. (Boekema et al., 2000) developed a nomenclature in which the PS II core (C), strongly (S), medium (M) and loosely (L) bound LHCII are denoted by the letters in brackets. The crystals with row spacings of 230 Å appear to correspond with the C_2S_2 LHCII-PS II complexes first reported in (Boekema et al., 1995) and which consist of a central core dimer flanked by two sets of strongly bound LHCII (Nield et al., 2000c). The more widely spaced crystalline arrays appear to contain C_2S_2M LHCII-PS II complexes which in addition to the C_2S_2 components appear to bind an additional LHCII trimer and CP24 (Lhcb6) subunit.

The abundance of 2D arrays of LHCII-PS II complexes in native membranes of higher plants suggests that they play an important functional role in vivo. As the complexes in these arrays are in close contact with one another, it is quite possible that the pigments that they bind are able to form an excitonically coupled network within the bilayer plane. The observation that a large number of the Chl molecules in LHCII and PS II are located towards the surface of the membrane-spanning domain and that 2D arrays of LHCII-PS II complex in adjacent granal membranes appear able to interlock structurally, opens up the possibility that these ordered macromolecular assemblies could transfer energy between adjacent membranes and therefore act as 3D excitonically coupled systems.

Under high light conditions PS II is susceptible to photodamage, which ultimately requires the D1 protein to be exchanged (Barber and Andersson, 1992). By excitonically coupling the antenna and reaction centers of PS II in this way, excess excitation energy at one point could be dissipated throughout the network and ultimately passed on to one of the non-excited reaction centers, thereby providing a greater degree of photoprotection than that afforded to non-arrayed complexes.

The unit cell dimensions of typical 2D arrays of LHCII-PS II supercomplexes are only large enough to accommodate approximately 100–140 Chl molecules per reaction center (Hankamer et al., 1997b), although it is estimated that the Chl:RC ratio in the grana membrane is about 250:1 (Lam et al., 1983). The additional Chls, which are probably associated with LHCII, must be accounted for. In this context it should be noted that the ratio of 250:1 is an average value and that the freeze etch images of (Seibert et al., 1987) clearly show that the grana contain a large proportion of non arrayed ESs particles. It is quite possible therefore that the non-arrayed PS II particles are associated with much larger antenna systems, or that a substantial pool of LHCII not associated with PS II exists in these parts of the grana, thus accounting for an overall average of ~250 Chl:RC. One possibility is that non-arrayed ESs particles with large antenna systems may be adapted to exciton trapping under low light conditions, with the arrayed particles providing a degree of photoprotection under high light conditions through a coupled Chl network. This general idea is supported by the fact that PS II complexes binding Lhcb1-6 can be isolated from detergent-solubilized PS II enriched granal membranes by sucrose density gradient centrifugation (Hankamer et al., 1997b). The non-arrayed ESs particles may also include a proportion of PS II subcomplexes containing damaged D1 which are in the processes of migrating to and from the stromal lamellae during the D1 repair cycle (Barbato et al., 1992; Zhang and Aro, 2002).

V. Future Prospects and Concluding Remarks

Although as yet there are no high-resolution X-ray structures of PS II from higher plants or green algae, this information will ultimately materialize. However, it will still be necessary to understand the structural information obtained in terms of PS II function within the thylakoid membrane and establish how the Chl *a/b* light harvesting systems couple to the PS II reaction center core and how, indeed, adjacent PS II megacomplexes associate with each other. All this will need to be understood against a backdrop

of PS II dynamics, including structural changes that occur during biogenesis, D1 turnover, state transitions, non-photochemical quenching and adaptation to different environmental conditions such as light intensities. Electron cryo-tomography, coupled with even higher resolution electron microscopy, as well as X-ray crystallography, will be able to address these challenges. The continuing efforts to obtain a higher resolution 3D structure of the LHCII-PS II supercomplex using single particle analysis and electron crystallography are a step towards the ultimate goal of describing not only how PS II of plants and green algae oxidize water, but also how they regulate this key reaction over a range of different environmental conditions.

Acknowledgments

We wish to thank the Biotechnology and Biological Sciences Research Council (BBSRC) for financial support. JN also acknowledges the Royal Society for supporting him as a University Research Fellow.

References

Adir N (1999) Crystallization of the oxygen-evolving reaction centre of Photosystem II in nine different detergent mixtures. Acta Crystallogr D Biol Crystallogr 55 (Pt 4): 891–894

Adir N, Dobrovetsky Y and Lerner N (2001) Structure of c-phycocyanin from the thermophilic cyanobacterium *Synechococcus vulcanus* at 2.5 Å: Structural implications for thermal stability in phycobilisome assembly. J Mol Biol 313: 71–81

Albertsson PA (1995) The structure and function of the chloroplast photosynthetic membrane — a model for the domain organization. Photosynth Res 46: 141–149

Albertsson PA, Yu SG and Larsson UK (1990) Heterogeneity in Photosystem II. Evidence from fluorescence and gel electrophoresis experiments. Biochim Biophys Acta 1016: 137–140

Anderson JM and Melis A (1983) Localization of different photosystems in separate regions of chloroplast membranes. Proc Natl Acad Sci USA 80: 745–749

Andersson B and Anderson JM (1980) Lateral heterogeneity in the distribution of chlorophyll-protein complexes of the thylakoid membranes of spinach chloroplasts. Biochim Biophys Acta 593: 427–440

Armond P, A. and Arntzen CJ (1977) Localization and characterization of PS II in grana and stroma lamellae. Plant Physiol 59: 398–404

Auer M, Scarborough GA and Kühlbrandt W (1999) Surface crystallisation of the plasma membrane H^+-ATPase on a carbon support film for electron crystallography. J Mol Biol 287: 961–968

Barbato R, Friso G, Rigoni F, Dalla Vecchia F and Giacometti GM (1992) Structural changes and lateral redistribution of Photosystem II during donor side photoinhibition of thylakoids. J Cell Biol 119: 325–335

Barber J (1980) An explanation for the relationship between salt-induced thylakoid stacking and the fluorescence changes associated with changes in spill-over energy from Photosystem II to Photosystem I. FEBS Lett 118: 1–10

Barber J (1982) Influence of surface charges on thylakoid structure and function. Ann Rev Plant Physiol 33: 261–295

Barber J (2003) Photosystem II: the engine of life. Q Rev Biophys 36: 71–89

Barber J and Andersson B (1992) Too much of a good thing: Light can be bad for photosynthesis. Trends Biochem Sci 17: 61–66

Barber J, Nield J, Morris EP, Zheleva D and Hankamer B (1997) The structure, function and dynamics of Photosystem two. Physiologia Plantarum 100: 817–827

Baumeister W, Grimm R and Walz J (1999) Electron tomography of molecules and cells. Trends Cell Biol 9: 81–85

Bibby TS, Mary I, Nield J, Partensky F and Barber J (2003a) Low-light-adapted *Prochlorococcus* species possess specific antennae for each photosystem. Nature 424: 1051–1054

Bibby TS, Nield J, Chen M, Larkum AW and Barber J (2003b) Structure of a Photosystem II supercomplex isolated from *Prochloron didemni* retaining its chlorophyll *a/b* light-harvesting system. Proc Natl Acad Sci USA 100: 9050–9054

Boekema EJ, Hankamer B, Bald D, Kruip J, Nield J, Boonstra AF, Barber J and Rögner M (1995) Supramolecular structure of the Photosystem II complex from green plants and cyanobacteria. Proc Natl Acad Sci USA 92: 175–179

Boekema EJ, van Roon H, Calkoen F, Bassi R and Dekker JP (1999a) Multiple types of association of Photosystem II and its light-harvesting antenna in partially solubilized Photosystem II membranes. Biochemistry 38: 2233–2239

Boekema EJ, Van Roon H, Van Breemen JF and Dekker JP (1999b) Supramolecular organization of Photosystem II and its light-harvesting antenna in partially solubilized Photosystem II membranes. Eur J Biochem 266: 444–452

Boekema EJ, van Breemen JF, van Roon H and Dekker JP (2000a) Arrangement of Photosystem II supercomplexes in crystalline macrodomains within the thylakoid membrane of green plant chloroplasts. J Mol Biol 301: 1123–1133

Boekema EJ, van Breemen JF, van Roon H and Dekker JP (2000b) Conformational changes in Photosystem II supercomplexes upon removal of extrinsic subunits. Biochemistry 39: 12907–12915

Böttcher B, Wynne SA and Crowther RA (1997) Determination of the fold of the core protein of hepatitis B virus by electron cryomicroscopy. Nature 386: 88–91

Brejc K, Ficner R, Huber R and Steinbacher S (1995) Isolation, crystallization, crystal structure analysis and refinement of allophycocyanin from the cyanobacterium *Spirulina platensis* at 2.3 Å resolution. J Mol Biol 249: 424–440

Büchel C, Morris E, Orlova E and Barber J (2001) Localisation of the PsbH subunit in Photosystem II: A new approach using labelling of His-tags with a $Ni^{(2+)}$-NTA gold cluster and single particle analysis. J Mol Biol 312: 371–379

Chen S, Roseman AM and Saibil HR (1998) Electron microscopy of chaperonins. Methods Enzymol 290: 242–253

Chiu W, McGough A, Sherman MB and Schmid MF (1999) High-resolution electron cryomicroscopy of macromolecular assemblies. Trends Cell Biol 9: 154–159

da Fonseca P, Morris EP, Hankamer B and Barber J (2002) Electron crystallographic study of Photosystem II of the cyanobacterium *Synechococcus elongatus*. Biochemistry 41: 5163–5167

De Las Rivas J, Balsera M and Barber J (2004) Evolution of oxygenic photosynthesis: Genome-wide analysis of the OEC extrinsic proteins. Trends Plant Sci 9: 18–25

Deisenhofer J, Epp O, Miki K, Huber R and Michel H (1984) X-ray structure analysis of a membrane protein complex. Electron density map at 3 Å resolution and a model of the chromophores of the photosynthetic reaction center from *Rhodopseudomonas viridis*. J Mol Biol 180: 385–398

Deng Y, Marko M, Buttle KF, Leith A, Mieczkowski M and Mannella CA (1999) Cubic membrane structure in amoeba (*Chaos carolinensis*) mitochondria determined by electron microscopic tomography. J Struct Biol 127: 231–239

DeRosier DJ and Klug A (1968) Reconstruction of three dimensional structures from electron micrographs. Nature 217: 130–134

Diner BA and Babcock GT (1996) Structure, Dynamics and Energy Conversion Efficiency in Photosystem II. In: Ort DR and Yocum CF (eds) Oxygenic Photosynthesis: The Light Reactions, pp 213–247. Kluwer Academic, Dordrecht

Dube P, Tavares P, Lurz R and van Heel M (1993) The portal protein of bacteriophage SPP1: A DNA pump with 13-fold symmetry. EMBO J 12: 1303–1309

Dubochet J, Adrian M, Chang JJ, Homo JC, Lepault J, McDowall AW and Schultz P (1988) Cryo-electron microscopy of vitrified specimens. Q Rev Biophys 21: 129–228

Ducret A, Muller SA, Goldie KN, Hefti A, Sidler WA, Zuber H and Engel A (1998) Reconstitution, characterisation and mass analysis of the pentacylindrical allophycocyanin core complex from the cyanobacterium *Anabaena* sp. PCC 7120. J Mol Biol 278: 369–388

Ferreira KN, Iverson TM, Maghlaoui K, Barber J and Iwata S (2004) Architecture of the photosynthetic oxygen-evolving coneter. Science 303: 1831–1838

Fotinou C, Kokkinidis M, Fritzsch G, Haase W, Michel H and Ghanotakis DF (1993) Characterization of a Photosystem-II core and its 3-D crystals. Photosynth Res 37: 41–48

Frank J (1980) The role of correlation techniques in computer image processing. In: Hawkes PW, Computer Processing of Electron Microscope Images, 187–222. Springer, Berlin

Fujiyoshi Y (1998) The structural study of membrane proteins by electron crystallography. Adv Biophys 35: 25–80

Green BR and Durnford DG (1996) The chlorophyll-carotenoid proteins of oxygenic photosynthesis. Ann Rev Plant Physiol 47: 685–714

Hankamer B, Barber J and Boekema EJ (1997a) Structure and Membrane Organization of Photosystem II From Green Plants. Annu Rev Plant Physiol Plant Molec Biol 48: 641–672

Hankamer B, Nield J, Zheleva D, Boekema E, Jansson S and Barber J (1997b) Isolation and biochemical characterisation of monomeric and dimeric Photosystem II complexes from spinach and their relevance to the organisation of Photosystem II in vivo. Eur J Biochem 243: 422–429

Hankamer B, Morris EP and Barber J (1999) Revealing the structure of the oxygen-evolving core dimer of Photosystem II by cryoelectron crystallography. Nat Struct Biol 6: 560–564

Hankamer B, Morris E, Nield J, Carne A and Barber J (2001a) Subunit positioning and transmembrane helix organisation in the core dimer of Photosystem II. FEBS Lett 504: 142–151

Hankamer B, Morris E, Nield J, Gerle C and Barber J (2001b) Three-dimensional structure of the Photosystem II core dimer of higher plants determined by electron microscopy. J Struct Biol 135: 262–269

Harauz G, Boekema E and van Heel M (1988) Statistical image analysis of electron micrographs of ribosomal subunits. Methods Enzymol 164: 35–49

Harrer R (2003) Associations between light-harvesting complexes and Photosystem II from *Marchantia polymorpha L.* determined by two- and three-dimensional electron microscopy. Photosynth Res 75: 249–258

Hasler L, Heymann JB, Engel A, Kistler J and Walz T (1998) 2D crystallization of membrane proteins: Rationales and examples. J Struct Biol 121: 162–171

Henderson R (1995) The potential and limitations of neutrons, electrons and X-rays for atomic resolution microscopy of unstained biological molecules. Q Rev Biophys 28: 171–193

Henderson R (2004) Realizing the potential of electron cryomicroscopy. Q Rev Biophys 33: 3–13

Henderson R, Baldwin JM, Downing KH, Lepault J and Zemlin F (1986) Structure of the purple membrane from *Halobacterium halobium* — recording, measurement and evaluation of electron micrographs at 3.5 Å resolution. Ultramicroscopy 19: 147–178

Henderson R, Baldwin JM, Ceska TA, Zemlin F, Beckmann E and Downing KH (1990) Model for the structure of bacteriorhodopsin based on high-resolution electron cryo-microscopy. J Mol Biol 213: 899–929

Henrysson T and Sundby C (1990) Characterisation of Photosystem II in stroma thylakoid membranes. Photosynth Res 25:

Hoenger A and Aebi U (1996) 3-D Reconstructions from ice-embedded and negatively stained biomacromolecular assemblies: A critical comparison. J Struct Biol 117: 99–116

Irrgang KD, Shi LX, Funk C and Schroder WP (1995) A nuclear-encoded subunit of the Photosystem II reaction center. J Biol Chem 270: 17588–17593

Jordan P, Fromme P, Witt HT, Klukas O, Saenger W and Krauss N (2001) Three-dimensional structure of cyanobacterial Photosystem I at 2.5 Å resolution. Nature 411: 909–917

Kamiya N and Shen JR (2003) Crystal structure of oxygen-evolving Photosystem II from *Thermosynechococcus vulcanus* at 3.7-Å resolution. Proc Natl Acad Sci USA 100: 98–103

Kargul J, Nield J and Barber J (2003) Three-dimensional reconstruction of a light-harvesting complex I-Photosystem I (LHCI-PS I) supercomplex from the green alga *Chlamydomonas reinhardtii*. J Biol Chem 278: 16135–16141

Kiselev NA, Sherman MB and Tsuprun VL (1990) Negative staining of proteins. Electron Microsc Rev 3: 43–72

Kruse O (2001) Light-induced short-term adaptation mechanisms under redox control in the PS II-LHCII supercomplex: LHC II state transitions and PS II repair cycle. Naturwissenschaften 88: 284–292

Kühlbrandt W (1992) Two-dimensional crystallization of membrane proteins. Q Rev Biophys 25: 1–49

Kühlbrandt W, Wang DN and Fujiyoshi Y (1994) Atomic model of plant light-harvesting complex by electron crystallography. Nature 367: 614–621

Kunji ER, von Gronau S, Oesterhelt D and Henderson R (2000) The three-dimensional structure of halorhodopsin to 5 Å by electron crystallography: A new unbending procedure for two-dimensional crystals by using a global reference structure. Proc

Natl Acad Sci USA 97: 4637–4642
Lam E, Baltimore B, Ortiz W, Chollar S, Melis A and Malkin R (1983) Characterization of a resolved oxygen-evolving photosystem-II preparation from spinach thylakoids. Biochim Biophys Acta 724: 201–211
Lebeau L, Lach F, Venien-Bryan C, Renault A, Dietrich J, Jahn T, Palmgren MG, Kühlbrandt W and Mioskowski C (2001) Two-dimensional crystallization of a membrane protein on a detergent-resistant lipid monolayer. J Mol Biol 308: 639–647
Levy D, Mosser G, Lambert O, Moeck GS, Bald D and Rigaud JL (1999) Two-dimensional crystallization on lipid layer: A successful approach for membrane proteins. J Struct Biol 127: 44–52
Liu Z, Yan H, Wang K, Kuang TY, Zhang J, Gul L, An X and Chang WR (2004) Crystal structure of spinach major light-harvesting complex at 2.72 Å resolution. Nature 428: 728–292
Mannella CA, Buttle K, Rath BK and Marko M (1998) Electron microscopic tomography of rat-liver mitochondria and their interaction with the endoplasmic reticulum. Biofactors 8: 225–228
Matadeen R, Patwardhan A, Gowen B, Orlova EV, Pape T, Cuff M, Mueller F, Brimacombe R and van Heel M (1999) The *Escherichia coli* large ribosomal subunit at 7.5 Å resolution. Structure Fold Des 7: 1575–1583
Miller K, R. (1981) Freeze-etching studies of photosynthetic membranes. In: Griffith JD (ed) Electron Microscopy in Biology, Vol 1, pp 1–30. Wiley-Interscience, New York
Miller KR, Miller GJ and McIntyre KR (1976) The light-harvesting chlorophyll-protein complex of Photosystem II. Its location in the photosynthetic membrane. J Cell Biol 71: 624–638
Miller KR and Cushman RA (1978) A chloroplast membrane lacking Photosystem II. Biochim Biophys Acta 546: 481–499
Mitsuoka K, Hirai T, Murata K, Miyazawa A, Kidera A, Kimura Y and Fujiyoshi Y (1999) The structure of bacteriorhodopsin at 3.0 Å resolution based on electron crystallography: Implication of the charge distribution. J Mol Biol 286: 861–882
Miyazawa A, Fujiyoshi Y, Stowell M and Unwin N (1999) Nicotinic acetylcholine receptor at 4.6 Å resolution: Transverse tunnels in the channel wall. J Mol Biol 288: 765–786
Miyazawa A, Fujiyoshi Y and Unwin N (2003) Structure and gating mechanism of the acetylcholine receptor pore. Nature 424: 949–955
Morris EP, Hankamer B, Zheleva D, Friso G and Barber J (1997) The three-dimensional structure of a Photosystem II core complex determined by electron crystallography. Structure 5: 837–849
Morschel EF and Schatz GH (1987) Correlation of Photosystem II complexes with exoplasmic freeze-fracture particles of cyanobacterium *Synechococcus* sp. Planta 172: 145–154
Murata K, Mitsuoka K, Hirai T, Walz T, Agre P, Heymann JB, Engel A and Fujiyoshi Y (2000) Structural determinants of water permeation through aquaporin-1. Nature 407: 599–605
Nicastro D, Frangakis AS, Typke D and Baumeister W (2000) Cryo-electron tomography of neurospora mitochondria. J Struct Biol 129: 48–56
Nield J, Funk C and Barber J (2000a) Supermolecular structure of Photosystem II and location of the PsbS protein. Philos Trans R Soc Lond B Biol Sci 355: 1337–1344
Nield J, Kruse O, Ruprecht J, da Fonseca P, Büchel C and Barber J (2000b) Three-dimensional structure of *Chlamydomonas reinhardtii* and *Synechococcus elongatus* Photosystem II complexes allows for comparison of their oxygen-evolving complex organization. J Biol Chem 275: 27940–27946
Nield J, Orlova EV, Morris EP, Gowen B, van Heel M and Barber J (2000c) 3D map of the plant Photosystem II supercomplex obtained by cryoelectron microscopy and single particle analysis. Nat Struct Biol 7: 44–47
Nield J, Balsera M, De Las Rivas J and Barber J (2002) Three-dimensional electron cryo-microscopy study of the extrinsic domains of the oxygen-evolving complex of spinach: Assignment of the PsbO protein. J Biol Chem 277: 15006–15012
Nield J, Rizkallah PJ, Barber J and Chayen NE (2003) The 1.45A three-dimensional structure of C-phycocyanin from the thermophilic cyanobacterium *Synechococcus elongatus*. J Struct Biol 141: 149–155
Nogales E, Wolf SG and Downing KH (1998) Structure of the alpha beta tubulin dimer by electron crystallography. Nature 391: 199–203
Olive J and Vallon O (1991) Structural organization of the thylakoid membrane: Freeze-fracture and immunocytochemical analysis. J Electron Microsc Tech 18: 360–374
Orlova EV (2000) Structural analysis of non-crystalline macromolecules: The ribosome. Acta Crystallogr D Biol Crystallogr 56 (Pt 10): 1253–1258
Orlova EV, Dube P, Harris JR, Beckman E, Zemlin F, Markl J and van Heel M (1997) Structure of keyhole limpet hemocyanin type 1 (KLH1) at 15 Å resolution by electron cryomicroscopy and angular reconstitution. J Mol Biol 271: 417–437
Perkins G, Renken C, Martone ME, Young SJ, Ellisman M and Frey T (1997) Electron tomography of neuronal mitochondria: Three-dimensional structure and organization of cristae and membrane contacts. J Struct Biol 119: 260–272
Perkins GA, Song JY, Tarsa L, Deerinck TJ, Ellisman MH and Frey TG (1998) Electron tomography of mitochondria from brown adipocytes reveals crista junctions. J Bioenerg Biomembr 30: 431–442
Radermacher M (1988) Three-dimensional reconstruction of single particles from random and nonrandom tilt series. J Electron Microsc Tech 9: 359–394
Reimer L (1997) Transmission Electron Microscopy: Physics of Image Formation and Microanalysis, Fourth edition. Springer Series in Optical Sciences, Vol 36. Springer, Berlin
Rhee KH (2001) Photosystem II: The solid structural era. Annu Rev Biophys Biomol Struct 30: 307–328
Rhee KH, Morris EP, Barber J and Kühlbrandt W (1998) Three-dimensional structure of the plant Photosystem II reaction centre at 8 Å resolution. Nature 396: 283–286
Ruprecht J and Nield J (2001) Determining the structure of biological macromolecules by transmission electron microscopy, single particle analysis and 3D reconstruction. Prog Biophys Mol Biol 75: 121–164
Saibil HR (2000a) Macromolecular structure determination by cryo-electron microscopy. Acta Crystallogr D Biol Crystallogr 56 (Pt 10): 1215–1222
Saibil HR (2000b) Conformational changes studied by cryo-electron microscopy. Nat Struct Biol 7: 711–714
Schatz M, Orlova EV, Dube P, Jager J and van Heel M (1995) Structure of *Lumbricus terrestris* hemoglobin at 30 Å resolution determined using angular reconstitution. J Struct Biol 114: 28–40
Schmidt-Krey I, Mitsuoka K, Hirai T, Murata K, Cheng Y, Fujiyoshi Y, Morgenstern R and Hebert H (2000) The three-

dimensional map of microsomal glutathione transferase 1 at 6 Å resolution. EMBO J 19: 6311–6316

Seibert M, DeWit M and Staehelin LA (1987) Structural localization of the O_2-evolving apparatus to multimeric (tetrameric) particles on the lumenal surface of freeze-etched photosynthetic membranes. J Cell Biol 105: 2257–2265

Sherman MB, Soejima T, Chiu W and van Heel M (1998) Multivariate analysis of single unit cells in electron crystallography. Ultramicroscopy 74: 179–199

Shi LX, Kim SJ, Marchant A, Robinson C and Schroder WP (1999) Characterisation of the PsbX protein from Photosystem II and light regulation of its gene expression in higher plants. Plant Mol Biol 40: 737–744

Simpson DJ (1978) Freeze-fracture studies on barley plastid membranes II. Wild-type chloroplast. Carlsberg Res Commun 43: 365–389

Simpson DJ (1979) Freeze-fracture studies on barley plastid membranes. III. Location of the light harvesting chlorophyll-protein. Carlsberg Res Commun 44: 305–336

Simpson DJ, Lindberg Moller B and Hoyer-Hansen G (1978) Freeze-fracture structure and polypeptide composition of thylakoids of wild type and mutant barley plastids. In: Akoyunoglou G ed) Chloroplast Development, pp 507–512. Elsevier/North-Holland Biomedical Press, Amsterdam

Staehelin LA (1976) Reversible particle movements associated with unstacking and restacking of chloroplast membranes in vitro. J Cell Biol 71: 136–158

Staehelin LA (1986) Chloroplast structure and supramolecular organization of photosynthetic membranes. In: Staehelin LA (ed) Photosynthesis III, Photosynthetic Membranes and Light Harvesting Systems, pp 1–84. Springer, Berlin

Stahlberg H, Braun T, de Groot B, Philippsen A, Borgnia MJ, Agre P, Kühlbrandt W and Engel A (2000) The 6.9-Å structure of GlpF: A basis for homology modeling of the glycerol channel from *Escherichia coli*. J Struct Biol 132: 133–141

Stowell MH, Miyazawa A and Unwin N (1998) Macromolecular structure determination by electron microscopy: New advances and recent results. Curr Opin Struct Biol 8: 595–600

Swiatek M, Kuras R, Sokolenko A, Higgs D, Olive J, Cinque G, Muller B, Eichacker LA, Stern DB, Bassi R, Herrmann RG and Wollman FA (2001) The chloroplast gene *ycf9* encodes a Photosystem II (PS II) core subunit, PsbZ, that participates in PS II supramolecular architecture. Plant Cell 13: 1347–1367

Tomo T, Enami I and Satoh K (1993) Orientation and nearest neighbor analysis of psbI gene product in the Photosystem II reaction center complex using bifunctional cross-linkers. FEBS Lett 323: 15–18

Tsvetkova NM, Apostolova EL, Brain APR, Williams WP and Quinn PJ (1995) Factors influencing PS II particle array formation in *Arabidopsis thaliana* chloroplasts and the relationship of such arrays to the thermostability of PS II. Biochim Biophys Acta 1228: 201–210

van Heel M (1986) Resolution criteria for three dimensional reconstruction. Optik 73: 119–122

van Heel M and Stoffler-Meilicke M (1985) Characteristic views of *E. coli* and *B. stearothermophilus* 30S ribosomal subunits in the electron microscope. EMBO J 4: 2389–2395

van Heel M (1987) Angular reconstitution: A posteriori assignment of projection directions for 3D reconstruction. Ultramicroscopy 21: 111–124

van Heel M, Schatz M and Orlova E (1992) Correlation functions revisited. Ultramicroscopy 46: 307–316

van Heel M, Gowen B, Matadeen R, Orlova EV, Finn R, Pape T, Cohen D, Stark H, Schmidt R, Schatz M and Patwardhan A (2000) Single-particle electron cryo-microscopy: Towards atomic resolution. Q Rev Biophys 33: 307–369

Vonck J (2000) Parameters affecting specimen flatness of two-dimensional crystals for electron crystallography. Ultramicroscopy 85: 123–129

Webber AN, Packman LC, Chapman DJ, Barber J and Gray JC (1989) The 5th chloroplast-encoded polypeptide is present in the photosystem-II reaction center complex. FEBS Lett 242: 259–262

Williams KA (2000) Three-dimensional structure of the ion-coupled transport protein NhaA. Nature 403: 112–115

Xu C, Rice WJ, He W and Stokes DL (2002) A structural model for the catalytic cycle of Ca(2+)-ATPase. J Mol Biol 316: 201–211

Zhang L and Aro E (2002) Synthesis, membrane insertion and assembly of the chloroplast-encoded polypeptide is present in the photosystem-II reaction center complex. FEBS Lett 512: 13–18

Zheleva D, Sharma J, Panico M, Morris HR and Barber J (1998) Isolation and characterization of monomeric and dimeric CP47-reaction center Photosystem II complexes. J Biol Chem 273: 16122–16127

Zouni A, Witt HT, Kern J, Fromme P, Krauss N, Saenger W and Orth P (2001) Crystal structure of Photosystem II from *Synechococcus elongatus* at 3.8 Ångstrom resolution. Nature 739–743